Effects of confinement on water structure and dynamics and on proton transport: a molecular simulation study

ARTICLE · JANUARY 2009

Source: OAI

1 AUTHOR:

Pussana Hirunsit

National Science and Technology Developm…

22 PUBLICATIONS **384** CITATIONS

SEE PROFILE

Effects of Confinement on Water Structure and Dynamics: A Molecular Simulation Study

P. Hirunsit and P. B. Balbuena*

Department of Chemical Engineering, Texas A&M University, College Station, Texas 77843

Received: June 14, 2006; In Final Form: September 24, 2006

Classical molecular dynamics simulations are performed to study structural and dynamic properties of water confined within graphite surfaces separated by a distance varying between 7 and 14.5 Å, at a constant water density of 1 g/cm^3. Results at 298 K show the formation of a well-ordered structure constituted by water layers parallel to the graphite surfaces. The water molecules in layers in contact with the surface have a tendency to orient their dipole parallel to the surface. Such ice-like structure may have, however, different structural and dynamical properties than those of ice. The time evolution of the calculated mean square displacement reveals that at the smallest separation (7 Å) the water mobility is significantly lower than that of low-temperature water (213 K) at the same density; the mobilities become similar at a separation of 8 Å although the structure of that confined water is very different from that in low-temperature water. The temperature at which the mobility of water confined between graphite walls separated at 7 Å would become similar to that in bulk low-temperature water was found to be 373 K. With respect to the dynamics of confined water, a significant blue shift is observed in the intermolecular vibrational modes associated with the O···O···O bending and O···O stretching of molecules linked by hydrogen bonds.

1. Introduction

The behavior of water confined in carbon nanostructures has many interesting implications in chemical, biological, and electrochemical fields, and several related applications have already been explored in the chemical, oil and gas, food, and pharmaceutical industries.[1] Our fundamental understanding of the behavior of confined water has been enriched by the study of water adsorption isotherms[2] and density distribution and water clustering growth[3] in carbon nanopores. Such behavior is influenced by water interactions with hydrophobic species in nanoenvironments such as those arising in water channels present in living organisms.[3,4] Furthermore, water in carbon nanotubes has been actively studied because its presence could alter the physical, chemical, and electronic properties of the nanotubes[5,6] which are sought as potential materials for electronics and biomedical devices.

Similarly to other systems in the nano regime, the structure and properties of water confined in nanoscale spaces may be very different from those of the bulk. X-ray diffraction experiments by Iiyama et al.[7,8] to determine the structure of a water molecular assembly in a hydrophobic nanospace with characteristic widths in the range of 1.13 nm between 148 and 303 K illustrated that confined water in carbon nanotubes shows solid-like structure. These authors showed that X-ray diffraction patterns of water adsorbed in slit-shaped carbon pores contain sharp peaks while there are no sharp peaks in the spectra of bulk liquid water. These sharp peaks suggest that the water molecules have an ordered, ice-like structure, which is plausible along the horizontal direction of the slit pore.[7] Experimental X-ray diffraction results also showed that the structure of water molecules confined in the same hydrophobic environment with pore widths of 0.75 nm at 303 K is more ordered compared with that of 1.3 nm without phase transition detected as a function of the pore size.[8] In addition, molecular simulations of the behavior of water encapsulated in carbon nanotubes were reported by Koga et al.[9] The simulations were performed with use of carbon nanotube diameters ranging from 1.1 to 1.4 nm and applied axial pressures of 50 to 500 MPa. The results showed the existence of a new ice phase, unlike any of the known bulk ice structures, which displayed a first-order transition to hexagonal and heptagonal ice nanotubes and a continuous phase transformation into solid-like square or pentagonal ice nanotubes.[9] Similarly, Striolo et al.[5] performed simulations of water in single-walled carbon nanotubes and observed layered ice-like structures.

One of the potential applications of the ice-type structures formed due to water confinement in hydrophobic structures is the use of these structures as proton-conductor media. Proton transport in aqueous solutions is fundamental to many biological and technological processes. Dellago et al.[10] have studied a system of proton transport along a single file of oriented water with hydrogen-bonding defects through water-filled carbon nanotubes using molecular dynamics (MD) simulations. They reported that charges and defects interact strongly, and such interaction causes them to diffuse together. The diffusion coefficient of the defect is of the order of 3−4 Å^2/ps, much lower compared with the proton diffusion constant of 17 Å^2/ps, when uncoupled from the motion of the defect. Moreover, Mann et al.[11] investigated proton transport along a one-dimensional water wire encapsulated inside (6,6) single-walled carbon nanotubes. Their simulation results suggested that a proton in the presence of neutral water tends to stay inside the carbon nanotubes rather than to achieve complete conduction through the nanotube interior. Instead, a proton rapidly diffuses from end to end under the presence of a small electric field applied along the carbon nanotube axis. These proton transport systems are believed to mediate proton conduction following a

* Address correspondence to this author. E-mail: balbuena@tamu.edu.

10.1021/jp063718v CCC: $37.00
Published on Web 01/10/2007

TABLE 1: LJ Potential Parameters for Carbon−Carbon (in Graphite) and Oxygen−Oxygen (in Water) Interactions

pair interaction	ϵ_{ij} (kcal/mol)	σ_{ij} (Å)
$O_{water}-O_{water}$[13]	0.1553	3.166
C−C[15]	0.0553	3.400

Grotthuss mechanism[12] involving proton hopping rather than molecular diffusion.

In this work, we focus on characterizing the structure and dynamics of water at room temperature and a density of 1 g/cm^3 within graphite walls of different separations, and on establishing differences between structural and dynamical properties of confined water and those of low-temperature water at the same density that could be useful to describe the environment in which a proton would move under these conditions.

2. Molecular Simulation Procedures

2.1. Force Fields. The simple point charge-extended (SCP/E) model is used for water.[13] The water model is represented as a sphere with an oxygen atom located in its center, and the hydrogen atoms 1.0 Å away, with an H−O−H angle of 109.5°. The charge on the oxygen site is −0.8476 and 0.4238 e on each of the hydrogen sites. Van der Waals interactions between atoms are described by a 12−6 Lennard-Jones (LJ) potential and the Ewald Sum technique is applied to account for the truncation of the long-range electrostatic forces.[14] The LJ potential function is

$$U(r_{ij}) = 4\epsilon_{ij}\left[\left(\frac{\sigma_{ij}}{r_{ij}}\right)^{12} - \left(\frac{\sigma_{ij}}{r_{ij}}\right)^{6}\right] \quad (1)$$

ϵ_{ij} and σ_{ij} are the LJ potential parameters that characterize the size and strength of the potential, and r_{ij} is the distance between the centers of mass of the pair atoms. The model parameters of the like interaction are given in Table 1, whereas those for the unlike interaction are calculated by the Lorentz−Berthelot combining rules:

$$\sigma_{ij} = \frac{\sigma_{ii} + \sigma_{jj}}{2}$$

$$\epsilon_{ij} = \sqrt{\epsilon_{ii}\epsilon_{jj}} \quad (2)$$

2.2. Building the System. To analyze the confinement effect of water between walls of a hydrophobic material, a graphite slab made of two layers was incorporated into the unit cell to simulate a slit pore containing water at 1 g/cm^3 and 298 K. The slit pore model is constructed such that graphite-like crystallites are semi-infinite and composed of two-layer graphite slabs aligned parallel to one another and separated by a distance H (Figure 1), which has been given values of 14.5, 11, 8, and 7 Å. The dimensions of the graphite slab are 17 × 19.68 Å^2. The volume of the system was calculated by excluding the volume occupied by the graphite slabs (Figure 1). Because of the periodic boundary conditions imposed on the system in the three spatial directions, water in the box is confined between the graphite slab in the bottom of the unit cell and the graphite slab located in the bottom of the next periodic cell. MD simulations are performed in the canonical NVT ensemble with the Evans thermostat,[14] using the DL_POLY program.[16] The equilibration time is set to be 300 ps and the time step 0.001 ps, with production times of 500 ps. After the system reaches equilibrium, the structural and dynamic properties are analyzed.

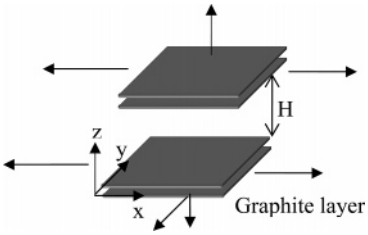

Figure 1. Schematic of the slit pore model.

2.3. Analysis of the Simulation Data. The structure is analyzed by using the pair radial distribution function, $g_{XY}(r)$, given by the ratio $\rho_{XY}(r)/\rho_{bulk}$, where $\rho_{XY}(r)$ is the local density of atoms Y located at position r from the center of atom X, ρ_{bulk} is the bulk density of atoms Y, and r is the radial distance measured in concentric spherical shells from the center of atom X.

The molecular diffusion is analyzed through the time evolution of the mean square displacement (MSD), a measure of the average distance that a molecule travels, which is defined as

$$\mathrm{MSD}(t) = \langle |r_i(t) - r_i(t_0)|^2 \rangle \quad (3)$$

with the quantity in broken brackets averaged over many different initial times t_0. The MSD of confined water molecules is computed in the ($x-y$) direction, according to

$$\mathrm{MSD}(t) = \langle |x_i(t) - x_i(t_0)|^2 + |y_i(t) - y_i(t_0)|^2 \rangle \quad (4)$$

The limiting slope of the MSD(t), considered for time intervals sufficiently long for it to be in the linear regime, is related to the self-diffusion constant D:

$$D = \frac{1}{\delta}\lim_{t\to\infty}\frac{\mathrm{d}\langle |r_i(t) - r_i(t_0)|^2 \rangle}{\mathrm{d}t} \quad (5)$$

where δ depends on the space dimensionality (6 for three dimensions, 4 for two dimensions).

3. Results and Discussion

MD simulations of bulk SPC/E water were performed at 1 g/cm^3 and at 213, 298, and 375 K. For the SPC/E model, the melting point of ice has been reported at 213 K.[17] The self-diffusion coefficients calculated according to eq 5 are 7.33 × 10^{-11}, 1.26 × 10^{-9}, 2.50 × 10^{-9}, and 7.45 × 10^{-9} m^2/s at 213, 270, 298, and 375 K, respectively. The calculated value at 298 K is fairly consistent with the experimental water self-diffusion coefficient of 2.30 × 10^{-9} m^2/s at 298.2 K.[18] SPC/E diffusion coefficients of low-temperature water have been reported in a wide range of temperatures and densities.[19] The calculated SPC/E diffusion coefficient at 210 K and at a density of 1 g/cm^3 is 1.03 × 10^{-11} m^2/s,[20] in fair agreement with our calculated value at 213 K. Simulations of hexagonal ice for the SPC/E model were reported by Trout et al.,[21] who determined a slope of 1.4 × 10^{-12} m^2/s for the MSD curve at 200 K. Using eq 5 this slope yields a diffusion coefficient of 2.3 × 10^{-13} m^2/s, 1 order of magnitude smaller with respect to that of low-temperature water at the same density (0.917 g/cm^3) and 210 K.[20] However, Trout et al.'s simulation was designed to measure the diffusion of interstitial water, and therefore, their final result is reported as the product of the calculated coefficient from eq 5 times the concentration of interstitial water molecules, yielding a much lower value of 1.3 × 10^{-18} m^2/s at 200 K and density of 0.917 g/cm^3. This last value is in good agreement with experiments by Goto et al.,[22] where an interstitial mechanism

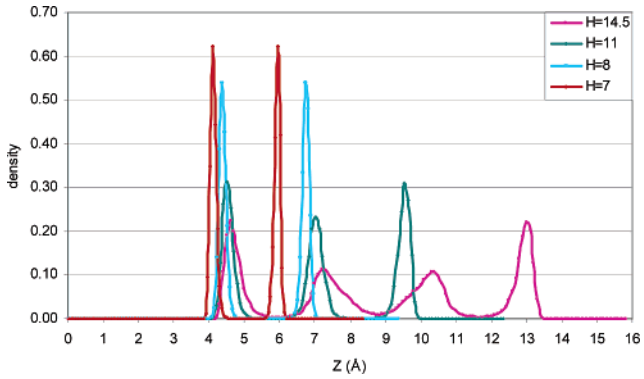

Figure 2. *Z*-density of oxygen atoms in water molecules at different separations *H* (in Å) between the walls of a slit pore, at 298 K. The walls are located at the left and right of the highest density peaks observed in the graph for each value of *H*. The separation between the first peak and the wall is approximately 2.7 Å for $H = 7$, 3 Å for $H = 8$, 3.1 Å for $H = 11$, and approximately 3.2 Å for $H = 14.5$ Å.

is proposed for the self-diffusion of water in ice. In this paper, we compare the dynamics of confined water with those of low-temperature water at the same density. For reference, in our discussion we also include the result of the MSD from ice (with density 0.917 g/cm^3) as obtained by Trout et al.[21]

Figure 2 shows the density profile of confined water at 1 g/cm^3 in a direction *Z* perpendicular to the graphite walls, which corresponds to the number density of oxygen atoms belonging to water molecules found in planes parallel to the graphite surfaces (*Z*-density). It is observed that there are four layers of water molecules distributed in the slit pore for $H = 14.5$ Å, three layers for $H = 11$ Å, and two layers at $H = 8$ and 7 Å.

Each of the profiles for a given value of *H* is symmetric; the highest peaks are always in contact with the walls, and their widths become sharper, solid-like, as *H* decreases (Figure 2). These observations are in agreement with other reports.[2,5,6,8,9,23]

The water structure illustrated in the snapshots shown in Figure 3 agrees with the experimental results carried out by Iiyama et al.,[7,8] who observed long-range well-ordered water molecules in the horizontal direction of a slit pore at room temperature.

Most of the water molecules located in the layers next to the walls orient with both of the hydrogen atoms located nearly in the same plane with its corresponding oxygen atom (Figure 3). Analysis of the density profiles shown in Figure 4 indicates that the distribution of hydrogen atoms in the water layers in contact with the surfaces is broader, therefore there are a number of hydrogen atoms located closer to the graphite surface than the corresponding oxygen atoms. On the contrary, there are a group of hydrogen atoms in the intermediate layers which are located farther from the graphite surfaces than their corresponding oxygen atoms. Similar results regarding the presence of H atoms closer to the walls were reported by other authors.[24,25] Pertsin and Grunze[25] incorporated H···C parameters in their Lennard-Jones potential, to match results of ab initio calculations, indicating that the most stable conformation of a water molecule in contact with graphite is that with a hydrogen atom pointing to the surface. We note, however, that such ab initio calculations result from the interaction of a single water molecule with a surface, which obviously will be greatly affected by the presence of other water molecules interacting strongly between them via hydrogen bonds.

In our simulations, even though the results agree with finding some H atoms closer to the walls, the interaction potential employed does not include H···C interactions. Note that Figure 4 shows that although hydrogen atoms in the layer adjacent to the graphite surface are found in positions closer than those of oxygen atoms, the peaks of oxygen and hydrogen atoms are nearly at the same position.

Thus, these results reveal that there are two preferential orientations of water molecules in the layer close to the

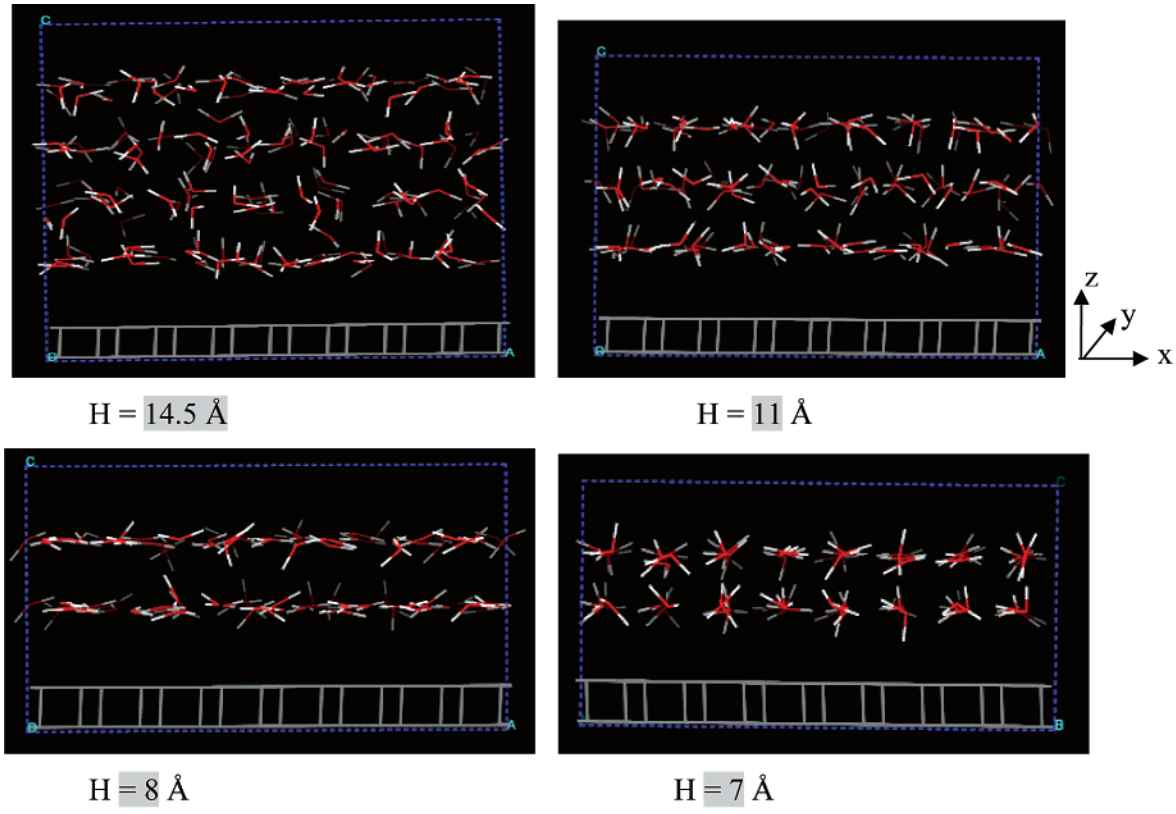

Figure 3. Snapshots of water molecules confined between graphite slabs where *H* is the separation between walls, at 298 K.

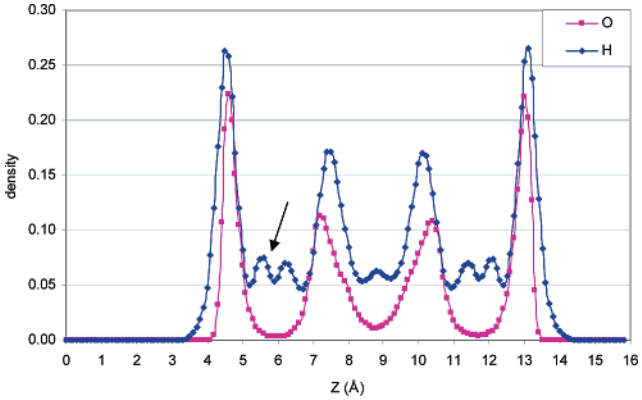

Figure 4. *Z*-density profiles of oxygen and hydrogen atoms of water molecules in a slit pore at $H = 14.5$ Å and 298 K. The walls are located at the left and right of the highest density peaks. The separation between the first peak and the wall is approximately 3.2 Å. Note that in the layers close to the wall, there are a small number of hydrogen atoms (represented by the small peak indicated by an arrow) located out of the plane where that water molecule resides. In the inner layers, a few H atoms are below the planes of their respective water molecules and most of the H atoms of those water molecules in the layer are above those planes, as shown by the peak of H atoms located shifted toward the center of the pore with respect to the peak of oxygen atoms in that layer. These results suggest that water molecules in contact with the carbon surface have a higher tendency to orient their dipole parallel to the surface.

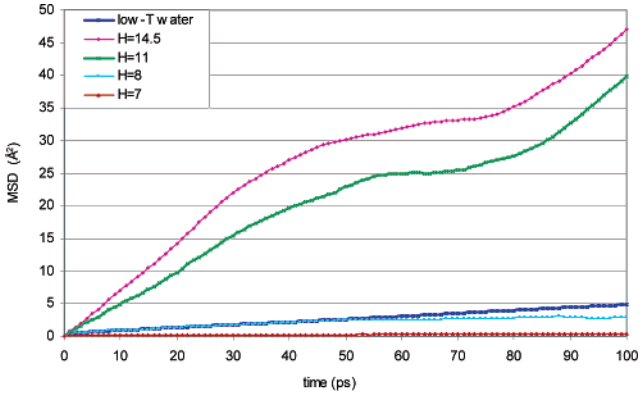

Figure 5. MSD of bulk low-temperature water (213 K) and confined water at different separations H (in Å) between the graphite layers at 298 K. The MSD of water in the $H = 8$ Å pore at 298 K is very similar to that of bulk low-temperature water (213 K). For reference, the diffusion coefficient calculated from the MSD for $H = 7$ Å is 7×10^{-13} m^2/s, of the same order of magnitude as that reported by Trout et al. for hexagonal ice (2.3×10^{-13} m^2/s).[21]

surfaces: the first one has both OH bonds parallel to the surface, and the second one has one OH pointing to the surface and the other parallel. Also, the first orientation is less frequently found in water molecules located in layers away from the graphite surface (i.e., in the center of the pore) where the interaction forces between the carbon surface and the water molecules become weakened as observed in Figure 3. Furthermore, the water molecules at the center of the pore prefer to orient maximizing the number of hydrogen bonds.

The confined water properties can be further investigated by analysis of a dynamic property, the MSD of oxygen atoms shown in Figure 5. The MSD of $H = 14.5$ Å is considerably higher than that of $H = 8$ Å. The water self-diffusion coefficient, given by eq 5, increases when H increases, in agreement with previous reports.[26] Interestingly, the MSD of low-temperature water at 213 K is very similar to the case of confined water at $H = 8$ Å. Note that at higher values of H ($H = 14.5$ Å, Figure 5), the average mobility is much higher than that of low-

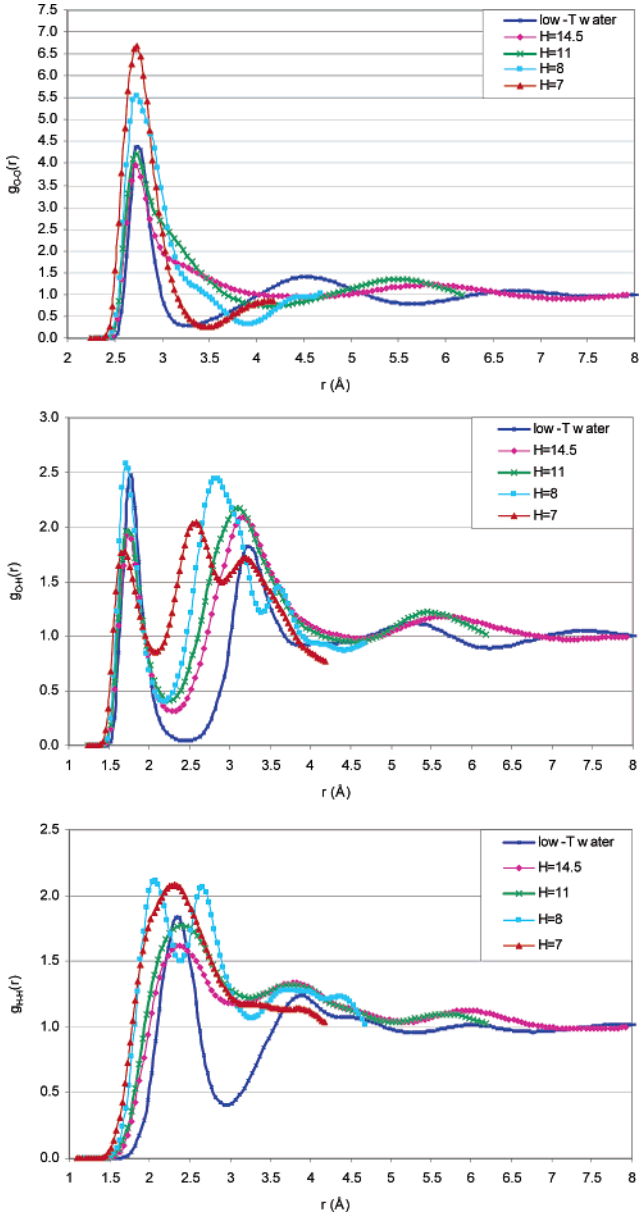

Figure 6. $g_{O-O}(r)$, $g_{O-H}(r)$, and $g_{H-H}(r)$ of low-temperature (213 K) and confined water (298 K) at various separations H (in Å) between the graphite walls.

temperature water, even though the layers close to the walls still maintain the frozen structure as shown in Figure 3. On the other hand, at the smallest separation, $H = 7$ Å, the average diffusion coefficient is much lower than that of low-temperature water at the same density of 1 g/cm^3, being of the same order of magnitude as that reported by Trout et al.[21] from simulations of SPC/E hexagonal ice at 0.917 g/cm^3 and 200 K.

These results imply that the mobility of water molecules significantly decreases under extreme confinement at $H \leq 8$ Å, in contrast to the persistent mobility reported by Leng and Cummings[26] for water between moving mica sheets, where the smallest size is 9.2 Å. Such a difference in dynamic behavior may be attributed not only to the different nature of the surfaces (hydrophilic vs hydrophobic) but also to the presence of an external field given by the shear force. Similarly, Kalra et al.[23] observed that a water layer confined between carbon nanotube membranes which are separated by a distance of approximately 3 Å still remains fluid while flowing through the membranes under an osmotic pressure gradient, and Vaiteheeswaran et al.,[27] who analyzed the effect of an applied electric field on the

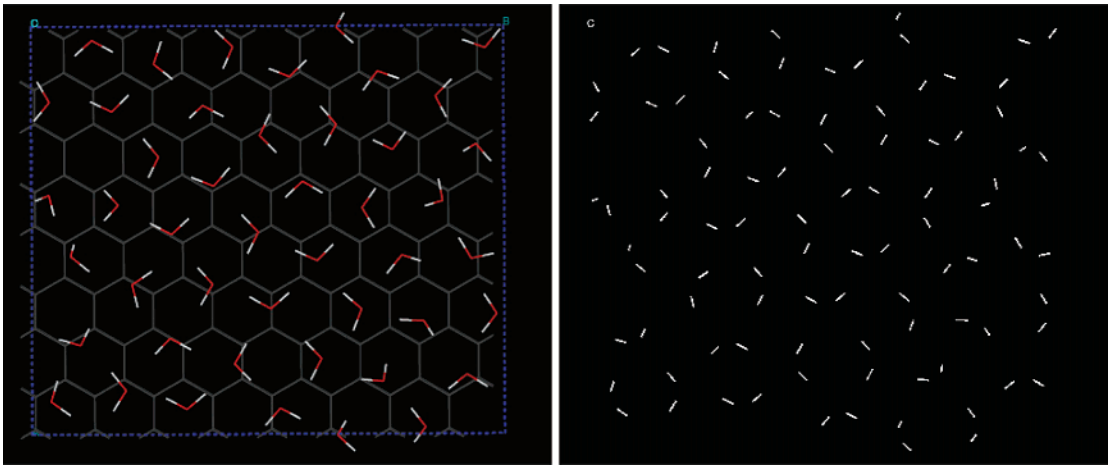

Figure 7. Snapshots of the water layer in contact with one of the walls for $H = 8$ Å. In the figure at the right, the background surface has been removed to visualize the order of the water structure.

structure of confined water between graphite walls, found that the density of the water film decreases and evaporation takes place. Definitely these external fields (in addition to the surface external potential exerted on the confined fluid) induce other effects in the system, but they cannot be directly compared with our results.

The structures shown by the radial distribution functions for low-temperature and confined water are substantially different (Figure 6). For example, the $g_{O-O}(r)$ for $H = 14.5$ and 11 Å have much broader first peaks which clearly show the departure from the ice tetrahedral structure. Starr et al.[20] proposed that the structure of low-temperature low-density water was similar to that of low-density amorphous (LDA) solid−water, consisting of an open tetrahedral network, whereas with increasing density the structure becomes closer to that of high-density amorphous (HDA) solid water, similar to water under pressure. The case that we are considering of density = 1 g/cm^3 is closer to the LDA system. Integration of the $g_{O-O}(r)$ until the minimum after the first peak yields 14 water molecules, whereas a value of 4 is obtained in the case of low-temperature water corresponding to four waters in a tetrahedral structure, each one participating in four H-bonds. Thus, the broad first peak in confined water includes molecules in a given layer plus those in the first neighbor layer(s). For $H = 8$ Å, the calculated number of water molecules in the first shell reduces to 10.

Figure 7 illustrates that the water molecules distribute approximately one per ring, i.e., each molecule has 6 nearest neighbors in the same layer. The measured separation between layers for $H = 8$ Å is 3.8 Å, which is the distance of the minimum after the first peak (Figure 6, top); therefore, the other four water molecules found in the first coordination shell must come from molecules temporarily residing in the interlayer, as illustrated by the snapshot in Figure 3. This structure (see the right image) resembles the "low-energy" amorphous phase described by Koga and Tanaka[28] (their Figure 5b), which may exist at low temperature and strong confinements (3 Å < H < 6 Å) according to the phase diagram reported by these authors.

Integration of the first peak of the $g_{O-H}(r)$ for low-temperature water yields two H atoms that are forming H-bonds with an oxygen atom; these are two of the four H-bonds in which the water molecule participates, the other two bonds result from the involvement of each of its H atoms with the O atoms of another two molecules. In confined water, integration of the first peak of the $g_{O-H}(r)$ also yields two H atoms. However, the tetrahedral arrangement is broken. The position of the first peak in the $g_{O-H}(r)$ shifts left as the confinement increases (1.78 Å in low-temperature water, 1.73 Å for $H = 14.5$ and 11 Å, 1.71 Å for $H = 8$, and 1.69 Å for $H = 7$ Å). The shorter the O···H distance in the H-bond, the stronger and more linear the H-bond structure (the OHO angle will tend to 180°). The layered structure and the distribution shown in Figure 7 determine also the broadening of the second peak in the $g_{O-H}(r)$, and induce large changes in the $g_{H-H}(r)$ (Figure 6).

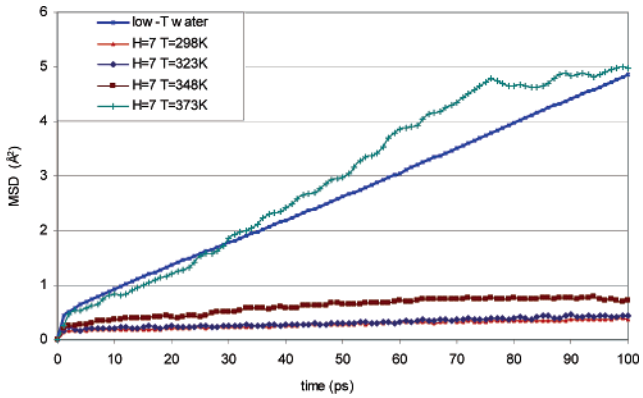

Figure 8. MSD of low-temperature water (213 K) and confined water in a pore of $H = 7$ Å at various temperatures.

We investigated at which temperature the water confined in the slit pores of $H = 7$ Å would have mobility comparable to that in low-temperature water. Figure 8 shows that the temperature has a mild effect on mobility in the confined system. At 323 and 348 K, the time evolution of the MSD yields nearly the same slope as that at room temperature, thus much lower mobility than bulk low-temperature water. It is at 373 K when the slope becomes similar to that in low-temperature water. This implies that the effect of the wall interaction exerted on confined water molecules produces a strong effect on the water dynamics, which is disrupted only at very high temperatures.

Further insights into the dynamics of the system are obtained by analysis of the normalized velocity autocorrelation function (vacf),[14] defined as

$$C_v(t) = \frac{\langle v_i(t) v_i(t_0) \rangle}{\langle v_i(t_0)^2 \rangle} \qquad (6)$$

where $v_i(t)$ is the velocity of O atoms in molecule i at time t, and the broken brackets indicate ensemble average over many initial times t_0. The vacf of water molecules is also computed in the lateral ($x-y$) direction. The results shown in Figure 9

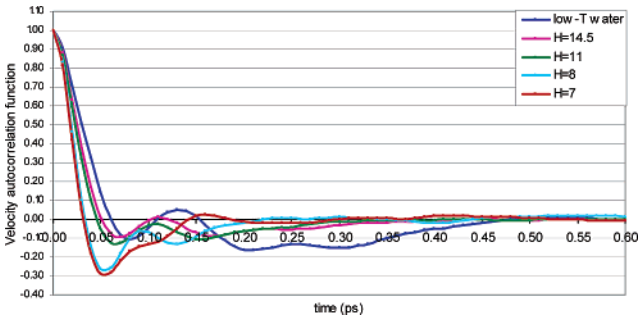

Figure 9. Velocity autocorrelation function of water molecules in low-temperature water, and that of water confined in slit pores separated by 7, 8, 11, and 14.5 Å, respectively.

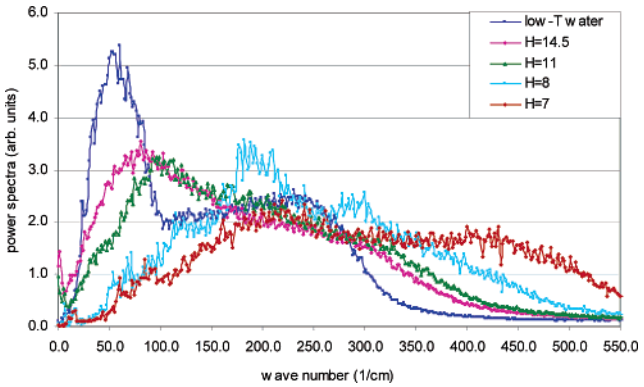

Figure 10. Power spectra obtained as the Fourier transform of the velocity autocorrelation function for water molecules in low-temperature water, and for water confined in slit pores separated by 7, 8, 11, and 14.5 Å, respectively.

again offer evidence of a clear difference between the dynamic behavior of bulk low-temperature water and confined water at the same density. The first minimum that corresponds to backscattering of the atoms becomes much deeper in the confined system as a consequence of its enhanced rigidity, as has been found in previous simulations of similar systems.[29] In the case of low-temperature water the first minimum is followed by an oscillation that is attributed to the intermolecular O−O stretch vibration, where the two water molecules are linked by an H-bond.[30] Figure 9 shows that for $H = 14.5$ Å, the vacf tends to become qualitatively similar to that of bulk water, but at stronger confinements the number of oscillations and the depth of the first minimum increase, signaling restricted molecular mobility.

Vibrational (power) spectra obtained by Fourier transforming the vacf are displayed in Figure 10. The spectrum corresponding to low-temperature water has two characteristic features: a peak at low frequencies (centered at ∼50 cm^{-1}), representing the O···O···O intermolecular bending motions of H-bonded molecules,[31] and a shoulder at ∼225 cm^{-1}, resulting from the O···O intermolecular stretching mode, also related to the H-bond in bulk water. Such a spectrum is substantially modified for confined water (Figure 10): the first peak has a blue shift (to higher frequencies), which becomes more pronounced as the separation between surfaces decreases. This may be another consequence of the distortion of the tetrahedral order caused by lateral diffusion being reduced and also by changes in the distribution of H-bonds. The blue shift was also observed in interfacial water present in micellar solutions.[31]

4. Conclusions

Water encapsulated in slit graphite pores calculated by MD simulations shows a well-ordered layered structure in the horizontal direction parallel to the graphite surfaces. When the surfaces are separated by distances lower than 8 Å, keeping the water density constant, a compact frozen structure composed of two layers is obtained, with mobility much lower than that of low-temperature water, where each water layer interacts strongly with its closest hydrophobic surface. Those water molecules in contact with the surface tend to orient their dipoles parallel to the surface. For larger separations additional water layers are formed in the pore center, and the average diffusion coefficient increases, becoming larger than that of low-temperature water for separations greater than 8 Å. At $H = 8$ Å, confined water has similar mobility as bulk low-temperature water (213 K), however, with very different structure. At $H = 7$ Å the water mobility is much lower than that of low-temperature water; such strong hydrophobic interaction between water molecules and graphite can be overcome by a large temperature increase. For example, the simulations indicate that the mobility of water molecules becomes similar to that in low-temperature water at 373 K in a pore of $H = 7$ Å. Structural and dynamical analyses suggest that the tetrahedral structure of low-temperature water is no longer present in the confined systems. Notable changes are observed in the intermolecular vibrational modes, mainly a blue shift of the O···O···O intermolecular bending motion that becomes more pronounced as the separation between walls becomes smaller, again signaling suppression of the tetrahedral order and increased system rigidity.

Acknowledgment. Financial support from the Army Research Office through contract DAAD 19-02-D-0001 is gratefully acknowledged. P.H. would like to thank the National Nanotechnology Center of Thailand for providing a scholarship.

References and Notes

(1) Brennan, J. K.; Bandosz, T. J.; Thomson, K. T.; Gubbins, K. E. Water in porous carbons. *Colloids Surfaces, A* **2001**, *187−188*, 539−568.

(2) Striolo, A.; Gubbins, K. E.; Chialvo, A. A.; Cummings, P. T. The Effect of Pore Connectivity on Water Adsorption Isotherms in Non-Activated Graphitic Nanopores. *Adsorption* **2005**, *11*, 337−341.

(3) Ohba, T.; Kanoh, H.; Kaneko, K. Water Cluster Growth in Hydrophobic Solid Nanospaces. *Chem. Eur. J.* **2005**, *11*, 4890−4894.

(4) Choudhury, N.; Pettitt, B. M. On the mechanism of hydrophobic association of nanoscopic solutes. *J. Am. Chem. Soc.* **2005**, *127*, 3556−3567.

(5) Striolo, A.; Chialvo, A. A.; Gubbins, K. E.; Cummings, P. T. Water in carbon nanotubes: Adsorption isotherms and thermodynamic properties from molecular simulation. *J. Chem. Phys.* **2005**, *122*, 234712.

(6) Striolo, A.; Naicker, P. K.; Chialvo, A. A.; Cummings, P. T.; Gubbins, K. E. Simulated Water Adsorption Isotherms in Hydrophilic and Hydrophobic Cylindrical Nanopores. *Adsorption* **2005**, *11*, 397−401.

(7) Iiyama, T.; Nishikawa, K.; Otowa, T.; Kaneko, K. An Ordered Water Molecular Assembly Structure in a Slit-Shaped Carbon Nanospace. *J. Phys. Chem* **1995**, *99*, 10075−10076.

(8) Iiyama, T.; Nishikawa, K.; Suzuki, T.; Kaneko, K. Study of the structure of a water molecular assembly in a hydrophobic nanospace at low temperature with in situ X-ray diffraction. *Chem. Phys. Lett.* **1997**, *274*, 152−158.

(9) Koga, K.; Gao, G. T.; Tanaka, H.; Zeng, X. C. Formation of ordered ice nanotubes inside carbon nanotubes. *Nature* **2001**, *412*, 802−805.

(10) Dellago, C.; Naor, M. M.; Hummer, G. Proton Transport through Water-Filled Carbon Nanotubes. *Phys. Rev. Lett.* **2003**, *90*, 105902.

(11) Mann, D. J.; Halls, M. D. Water Alignment and Proton Conduction inside Carbon Nanotubes. *Phys. Rev. Lett.* **2003**, *90*, 195503.

(12) Agmon, N. The Grotthuss mechanism. *Chem. Phys. Lett.* **1995**, *244*, 456−462.

(13) Berendsen, H. J. C.; Grigera, J. R.; Straatsma, T. P. The missing term in effective pair potentials. *J. Phys. Chem.* **1987**, *91*, 6269−6271.

(14) Allen, M. P.; Tildesley, D. J. *Computer Simulation of Liquids*; Oxford University Press: Oxford, UK, 1990.

(15) Steele, W. A. *The Interaction of Gases with Solid Surfaces*; Pergamon Press: Oxford, UK, 1974.

(16) Smith, W.; Forester, T. R. DL_POLY; Daresbury Laboratory: Daresbury, 1996.

(17) Garcia-Fernandez, R.; Abascal, J. L. F.; Vega, C. The melting point of ice I_h for common water models calculated from direct coexistence of the solid−liquid interface. *J. Chem. Phys.* **2006**, *124*, 144506.

(18) Krynicki, K.; Green, C. D.; Sawyer, D. W. Pressure and temperature dependence of self-diffusion in water. *Faraday Discuss. Chem. Soc.* **1978**, *66*, 199−208.

(19) Netz, P. A.; Starr, F. W.; Stanley, H. E.; Barbosa, M. C. Static and dynamic properties of stretched water. *J. Chem. Phys.* **2001**, *115*, 344−348.

(20) Starr, F. W.; Sciortino, F.; Stanley, H. E. Dynamics of simulated water under pressure. *Phys. Rev. E* **1999**, *60*, 6757.

(21) Demurov, A.; Radhakrishnan, R.; Trout, B. L. Computations of diffusivities in ice and CO_2 clathrate hydrates via molecular dynamics and Monte Carlo simulations. *J. Chem. Phys.* **2002**, *116*, 702−709.

(22) Goto, K.; Hondoh, T.; Higashi, A. Determination of self-diffusion coefficients of self-interstitials in ice with a new method of observing climb of dislocations by X-ray topography. *Jpn. J. Appl. Phys.* **1986**, *25*, 351−357.

(23) Kalra, A.; Garde, S.; Hummer, G. Osmotic water transport through carbon nanotube membranes. *PNAS* **2003**, *100*, 10175−10180.

(24) Marty, J.; Nagy, G.; Gordillo, M. C.; Guardia, E. Molecular simulation of liquid water confined inside graphite channels: Thermodynamics and structural properties. *J. Chem. Phys.* **2006**, *124*, 094703.

(25) Pertsin, A.; Grunze, M. Water-Graphite Interaction and Behavior of Water Near the Graphite Surface. *J. Phys. Chem. B* **2004**, *108*, 1357−1364.

(26) Leng, Y.; Cummings, P. T. Fluidity of Hydration Layers Nanoconfined between Mica Surfaces. *Phys. Rev. Lett.* **2005**, *94*, 026101.

(27) Vaitheeswaran, S.; Yin, H.; Rasaiah, J. C. Water between plates in the presence of an electric field in an open system. *J. Phys. Chem. B* **2005**, *109*, 6629−6635.

(28) Koga, K.; Tanaka, H. Phase diagram of water between hydrophobic surfaces. *J. Chem. Phys.* **2005**, *122*, 104711.

(29) Lee, S. H.; Rossky, P. J. A comparison of the structure and dynamics of liquid water at hydrophobic and hydrophilic surfaces−a molecular dynamics simulation study. *J. Chem. Phys.* **1994**, *100*, 3334−3345.

(30) Stillinger, F. H.; Rahman, A. Improved simulation of water by molecular dynamics. *J. Chem. Phys.* **1974**, *60*, 1545.

(31) Pal, S.; Balasubramanian, S.; Bagchi, B. Dynamics of bound and free water in an aqueous micellar solution: Analysis of the lifetime and vibrational frequencies of hydrogen bonds at a complex interface. *Phys. Rev. E* **2003**, *67*, 061502.